Effects of magnetic field and optical fluence on terahertz emission in gallium arsenide

A. Corchia,[1,2*] R. McLaughlin,[1,2] M. B. Johnston,[1] D. M. Whittaker,[2] D. D. Arnone,[2] E. H. Linfield,[1] A. G. Davies,[1] and M. Pepper[1,2]

[1]*Cavendish Laboratory, University of Cambridge, Madingley Road, Cambridge CB3 0HE, United Kingdom*

[2]*Toshiba Research Europe Limited, Cambridge Research Laboratory, 260 Cambridge Science Park, Milton Road, Cambridge CB4 0WE, United Kingdom*

(Received 23 March 2001; revised manuscript received 9 August 2001; published 26 October 2001)

The excitation density dependence of magnetic-field-enhanced terahertz (THz=10^{12} Hz) emission from (100) GaAs is studied. It is found that THz power saturates at a higher optical-excitation density, when a magnetic field is applied. This observation explains the different magnetic field enhancements that have been reported recently. At low excitation densities the results are shown to be consistent with a simple model of carrier-carrier scattering, whilst at higher densities surface field screening becomes important.

DOI: 10.1103/PhysRevB.64.205204 PACS number(s): 78.20.−e, 73.20.Mf, 76.40.+b, 78.47.+p

Emission of coherent radiation has been achieved in the ''terahertz gap'' (0.1–20 THz) by using semiconductors excited with subpicosecond pulses of interband (near-infrared or visible) light.[1,2] However, the need for brighter THz sources has recently been illustrated by the demonstration of biomedical applications of THz imaging,[3,4] which stand together with traditional and well-developed applications within solid-state physics, such as THz spectroscopy.[5] In order to achieve greater THz power, the physical mechanisms limiting the efficiency of visible-to-THz conversion must be understood and means for suppressing these mechanisms developed.

THz radiation can be generated at semiconductor surfaces by optical rectification,[6] lateral photocurrents in antennaes[1] or using surface-field photocurrents.[7] In the latter case, THz radiation is emitted when a photogenerated charge is accelerated by the surface-depletion electric field found at an air-semiconductor interface; the resulting transient photocurrent radiates at THz frequencies. Many studies have shown that, in a surface electric field, the total THz generated can be significantly enhanced by application of a magnetic field,[8–11] but the origin of this enhancement has only been clarified recently.[12,13] It has been demonstrated that the critical effect of the magnetic field consists of a change in the direction of the carrier acceleration.[12] Owing to the strong dielectric contrast typically found at a semiconductor surface, this change of direction determines a significant enhancement in the transmission of the radiated THz field through the air-semiconductor interface. Thus, the observed magnetic-field-induced increase in the emitted THz power results from a more efficient coupling of the THz radiation out of the sample.

Here, an experimental study of the magnetic-field-induced enhancement of THz emission from (100) GaAs is presented together with a model of the THz generation process. We find that the effect of the magnetic field on the carrier dynamics depends critically on the optical (interband) excitation density. This demonstrates that the magnetic-field-induced enhancement also varies significantly with the excitation density—a point not fully investigated in previous studies—and explains the discrepancies among different reported experimental studies.[8,9,14] We demonstrate that at low excitation densities, enhancement is limited by decoherence of the THz radiation induced by carrier-carrier scattering. Further, at high-excitation densities, experimental data and Monte Carlo simulations indicate that the magnetic field induces a reduction in the screening of the surface field.

The experimental apparatus used for this work has been described in detail elsewhere[8]. Briefly, a Ti:sapphire modelocked laser is used to produce optical pulses with a repetition rate of 87 MHz. The pulse duration is 130 fs with central wavelength at 760 nm. The laser beam is focused on a spot of diameter $\sim 600\ \mu$m and illuminates the sample, mounted in a cryostat, at an incidence angle of 45° [see Fig. 3(a)]. The maximum optical excitation power is ~ 180 mW (optical fluence $=0.2\ \mu$J cm^{-2} per pulse). The sample is an *n*-type (100)-oriented GaAs epilayer of 10-μm thickness grown on an undoped GaAs substrate: the carrier concentration is 1.2×10^{15} cm^{-3} and mobility 7.7×10^{4} cm^2 V^{-1} s^{-1} at 77 K. A magnetic field (B) between 0 and 8 T is applied orthogonal to the incident visible beam and parallel to the emitted THz beam. The emitted radiation is collected and focused onto a He-cooled bolometer by means of off-axis parabolic mirrors.

The THz emission measured in the presence of a variable magnetic field is reported in Fig. 1. Data refer to a temperature of 200 K and an excitation density of $n\sim1\times10^{16}$ cm^{-3} (fluence ~ 210 nJ cm^{-2}). As expected from the geometry of the experiment,[7] at $B=0$ T, the radiation is completely TM polarized . As the magnetic field increases, a TE component arises increasing faster than the TM component and reaching a maximum near 4 T, while the TM component increases monotonically up to ~ 6 T and then reaches a plateau. It is worth stressing, however, that significantly different trends have been reported in literature for the THz emission from GaAs and InAs in the presence of a magnetic field,[8,9,14] with critical parameters, such as the B value for maximum THz emission and for saturation, not being consistent among different studies. Interestingly, we find that the dependence of THz emission on the applied magnetic field varies critically with the excitation density. Thus, we ascribe these inconsistencies to different excitation regimes being used in the different experimental studies.

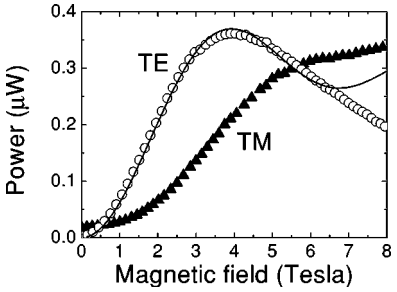

FIG. 1. THz radiation from (100) GaAs as a function of the applied magnetic field ($T=200$ K). Circles and triangles represent TE- and TM-polarized emitted power, respectively. Solid line is a fit to TE data (circles) from Eq. (3) with $b=0.8$.

Data shown in Fig. 2 clearly demonstrate the critical effect of excitation density on the magnetic-field-induced enhancement in GaAs. The TM- and TE-radiated THz power is measured for different magnetic fields and a variable excitation density, in the range 10^{14}-10^{16} cm^{-3}. For the TM component (top graph), the radiated power increases monotonically with B all over the excitation range, but for high excitation densities (typically $n>10^{15}$ cm^{-3}) the B-induced enhancement becomes larger. Moreover, in the high-excitation regime, a clear saturation of the radiated power is observed, which is stronger for lower magnetic-field values. This saturation effect, which is also present for the TE-radiated power, is discussed in the final section of the paper with the aid of a Monte Carlo simulation. The effect of excitation density on the TE-radiated power, plotted in the bottom graph of Fig. 2, is even more important. Moving from the low to the high excitation regime, the dependence of THz emission on the magnetic field varies significantly. For $n<2\times10^{15}$ cm^{-3}, THz power is approximately constant for 2 T$\leq B\leq$4 T and decreases for higher magnetic fields. For higher excitation densities, the power radiated at 2 T saturates strongly and becomes smaller than the power at $B\geq 6$ T: in this regime the emission peaks strongly at 4 T. These results are consistent with the measurements presented in

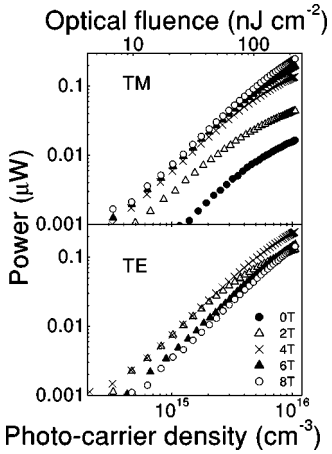

FIG. 2. Excitation density dependence of the TM (top graph) and TE (bottom graph) THz power radiated at 0 T (solid circles), 2 T (empty triangles), 4 T (crosses), 6 T (solid triangles), and 8 T (empty circles).

Fig. 1 ($n\sim1\times10^{16}$ cm^{-3}), which shows a maximum in TE power at 4 T. These experimental observations prove the critical role of excitation density in the B-induced enhancement of THz emission. Thus, in the following, we focus our analysis on the effect of excitation density on the carrier dynamics, which is responsible for the emission of THz radiation in the presence of a magnetic field.

In order to study the physical process induced by the magnetic field, we consider the motion of carriers under the combined effect of the intrinsic surface field and the applied magnetic field. In the absence of a magnetic field ($B=0$ T), the carriers photogenerated at the surface accelerate along the surface normal and acquire a *drift* velocity parallel to the surface electric field. Because the electric component of the far-field radiation emitted from an accelerated particle is proportional to the carrier acceleration,[15] the radiated field at $B=0$ T is TM polarized.[7] A magnetic field induces a cyclotron-like motion[16] in the plane orthogonal to B and changes the direction of the carrier acceleration, resulting in an additional contribution to both the TM and TE polarizations. Figure 3(b) illustrates the motion of a carrier in the plane orthogonal to the magnetic field. The carriers initially move along cyclotron orbits of radius r_c with angular velocity $\omega_c=eB/m^*$, where m^* is the carrier effective mass. The average diameter of the orbit is determined by the kinetic energy of the carriers associated with their drift motion in the surface field (E), namely, by the drift velocity. In the depletion region, this velocity is two orders of magnitude larger than the thermal velocity. In this process, one of the main limitations on THz emission is decoherence of the emitted radiation owing to scattering of the accelerated carrier. Because of their fast time scale (typically 100 fs[17,18]) optical-phonon scattering and carrier-carrier scattering are likely to be the most significant limiting processes. In the following, we will assume that the latter is predominant. We will then justify this assumption by comparing this model to our experimental observations. Carrier thermal motion induces a carrier-carrier collision after an average scattering time τ, which depends on the excitation carrier density (n) and the thermal energy. For the density range used ($n=10^{14}$-10^{16} cm^{-3}), Coulomb screening between electrons is significant and, as a result, carrier-carrier scattering is restricted to nearest-neighbor interactions only.[19] Consequently, we expect the scattering time to scale as the average distance between nearest-neighbor carriers[19] that are undergoing collective cyclotron motion, i.e., $d=n^{-1/3}$, instead of being proportional to n^{-1}, as observed in a Drude model in a hard-spheres approximation.[20] Thus, we define the carrier-carrier scattering time as

$$\tau=b\frac{n^{-1/3}}{\nu_{th}}, \tag{1}$$

where $\nu_{th}=(3k_BT/m^*)^{1/2}$ is the carrier thermal velocity and b is a proportionality constant. Between two collisions, a carrier travels over a portion of the cyclotron orbit (λ in Fig. 3b) corresponding to a ''scattering angle:''

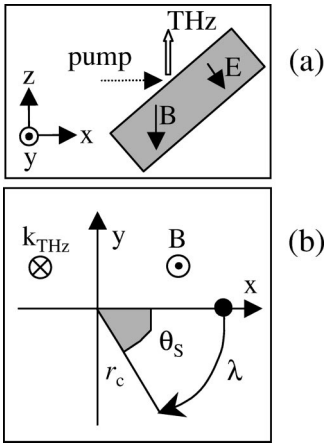

FIG. 3. (a) Orientation of the sample with respect to the exciting visible beam and applied magnetic field. (b) Motion of the carrier (black circle) in the plane orthogonal to the magnetic field (B): r_c is the average radius of the carrier orbit, λ indicates the scattering length, and θ_S is the scattering angle.

$$\theta_S(n,B)=\omega_c\tau=b\frac{eB}{m^*}\frac{n^{-1/3}}{\nu_{th}}. \tag{2}$$

Equations (1) and (2) show that as the applied magnetic field is increased (at a constant excitation density), both ω_c and θ_S increase (see Fig. 6) and so the carrier completes a larger portion of the orbit with higher acceleration. In the geometry of our experiment [see Fig. 3(b)], the carrier centripetal acceleration rotates in the x-y plane, orthogonal to the plane of incidence. Thus, it radiates both a TM and a TE component, parallel to x and y, respectively, while the drift acceleration in the x-z plane only emits a TM field. The relative contribution to the TM radiated field from the drift acceleration (orthogonal to the surface) and the cyclotron acceleration (at 45° to the surface) changes with B. Monte Carlo simulations[13] demonstrate that, since the drift and cyclotron accelerations have a different orientation with respect to the surface, the transmission of the corresponding radiated TM power at the air-semiconductor interface also changes with the applied magnetic-field. Thus, the magnetic field dependence of the TM component is significantly affected by the dielectric contrast at the semiconductor surface, while for the TE component this only results in a scaling factor independent of B. Thus here we analyze the TE component only, as it gives a direct measure of the rotation of the carrier acceleration. Taking the instantaneous THz field[10] and calculating the time-averaged power, we obtain for the magnetic-field-induced TE radiation:

$$P^{TE}(n,B)\propto\frac{n^2E^2}{m^2}\times\left[1-\frac{\sin 2\theta_S}{2\theta_S}\right]. \tag{3}$$

Equation (3) describes the THz power dependence on both applied magnetic field B and photogenerated carrier density n. When the magnetic field is varied, the second term in brackets in Eq. (3) modulates the emitted THz power around an asymptotic value, which depends on the strength of the surface field and on the excitation density (n). However, for an ensemble of electrons with a thermally broadened velocity distribution, the measured output power is given by an average of P^{TE} [Eq. (3)] over a distribution of different values for θ_S. Such a distribution smooths the sinusoidal oscillation predicted by Eq. (3).

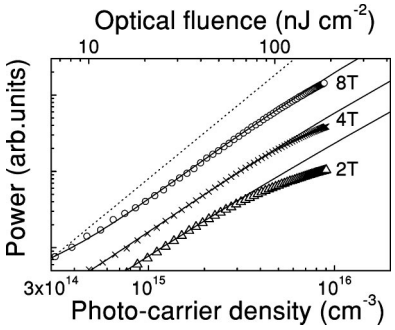

FIG. 4. Excitation density dependence of the TE THz power: fits (solid lines) to experimental data (symbols) for $B=2$ T, 4 T, and 8 T are obtained from Eq. (3) with $b=0.8$. Curves are offset for clarity. Dotted line represents a square dependence (slope=2) on the photocarrier density.

When the photogenerated carrier density n is increased for a given magnetic field, the scattering angle θ_S decreases (see Fig. 6) because the carrier-carrier scattering rate increases. As a result, the dependence of the emitted THz power on the excitation density in Eq. (3) deviates from a square power (expected in the absence of any scattering and screening effects). It is worth stressing at this point that screening of the surface field by moving charges is not taken into account here. As a consequence, the formulas we have derived do not describe the screening-induced saturation effects, which are observed experimentally at high excitation densities (see discussion of Fig. 4).

Equation (3) has been used to fit experimental data in Fig. 1 and Fig. 4 with b, introduced in Eq. (1), as a fit parameter.

In Fig. 1, showing the B dependence of THz power, the quality of the fit (solid line) to TE experimental data (circles) is good for magnetic fields up to ~6 T. The deviation of experimental data from our model at higher magnetic fields is due to the fact that, experimentally, electrons scatter at different angles according to their velocity distribution, while in the fitting function a single value of θ_S has been considered. Moreover, in Fig. 1 an excitation density $n\sim1\times10^{16}$ cm^{-3} was used. As shown in Fig. 2, this excitation density leads to appreciable screening of the surface field [not included in Eq. (3)] and contributes to the deviation of experimental data from the model.

The dependence of the TE-radiated power on the excitation density (described in details with Fig. 2) can also be modelled with Eq. (3). For clarity, only the experimental data and corresponding fitting curves for $B=2$, 4, and 8 T are shown in Fig. 4. The quality of the fit is very good in the low-excitation density regime up to $\sim2\times10^{15}$ cm^{-3} (fluence~100 nJ cm^{-2}) for $B=2$ T and to higher densities for higher magnetic fields. This confirms the assumption used in deriving Eq. (3), that carrier-carrier collisions are the main scattering event. If instead optical-phonon scattering

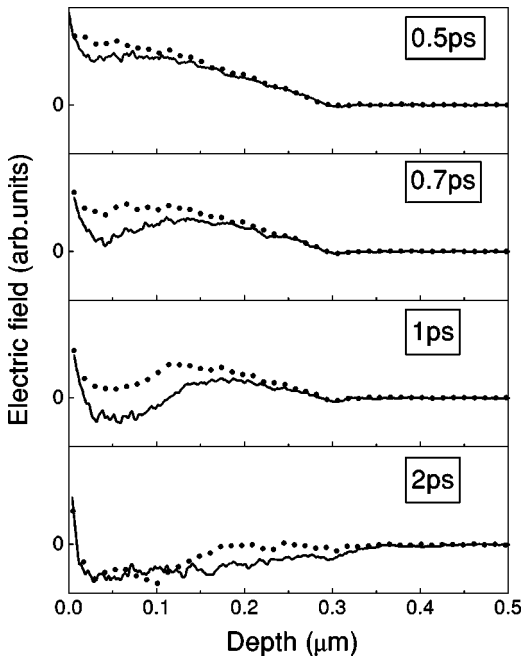

FIG. 5. Monte Carlo simulation of the surface electric field after photoexcitation ($t=0$ ps). Solid and dotted lines refer to an applied magnetic field of 0 T and 8 T.

was predominant, then its scattering rate, and the scattering angle θ_S defined in Eq. (2), would be independent of the density of carriers. As a consequence, the radiated THz power described by Eq. (3) would increase as the square power of the carrier density. However, our experimental data clearly show that this is not the case. The dotted curve in Fig. 4 indicates a square power trend (slope=2 in the plot): when comparing it to experimental data, it is clear that these have a weaker dependence on the photogenerated carrier density, even for the lowest excitation density range, where screening-induced saturation should not be significant. Conversely, when the carrier-carrier scattering rate is used to model the radiated power, as in Eq. (3) in our model, a good agreement with experimental data is achieved. Thus, we conclude that in the physical process leading to the emission of THz radiation, carrier-carrier scattering is the dominant scattering mechanism.

However, in spite of the effectiveness of the model, deviations do occur at higher-optical excitation densities owing to screening-induced saturation of the THz emitted power [not taken into account in formulas (1)–(3)]. When the density of the photogenerated carriers is comparable to that of the *doping* carrier density ($n_{dop}=1.2\times10^{15}$ cm^{-3}), the screening of the surface field by moving charges is expected to become significant and dampen the carrier acceleration. Figure 4 demonstrates this explicitly. For high-excitation densities, this effect counteracts the increase in photocurrent (expected as n increases) and makes the THz emission mechanism less efficient. Interestingly, the higher the applied magnetic field, the weaker is the screening-induced saturation: 2 T data in Fig. 4 deviate from the fitting curve for a photocarrier density of about 4×10^{15} cm^{-3}, while at $B=4$ T the ''saturation density'' is almost doubled.

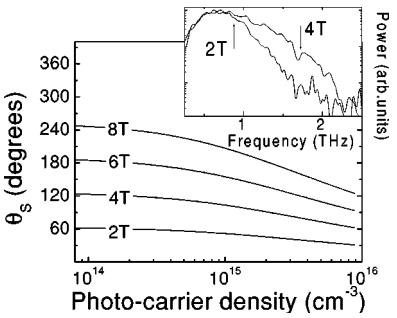

FIG. 6. The scattering angle θ_S is plotted as a function of the excitation density for different applied magnetic fields. θ_S is calculated from Eq. 2 with $b=0.8$, as inferred from experimental data. In the inset, experimental EOS spectra are shown for an applied magnetic field of 2 T and 4 T; arrows indicate the corresponding cyclotron frequency.

Monte Carlo simulations confirm this experimental observation.[13] Here, the mechanism of *surface-field photoconduction* has been modeled by using classical equations of motion for charged particles in a self-consistent electric field and a constant magnetic field. The key features of the simulation are: (a) the motion of holes is not included and their contribution to the photocurrent is neglected (because of their heavier effective mass); (b) screening of the *built-in* surface field by moving electrons is considered; (c) in a ''hot-electrons'' picture[17] the carrier mobility is assumed to be mainly limited by carrier-carrier scattering for the first few picoseconds after photoexcitation. In Fig. 5, the simulated time evolution of the surface electric field is shown. Solid and dashed lines refer to applied magnetic fields of 0 and 8 T, respectively. Up to 1 ps after photoexcitation, the simulation clearly shows that the surface electric field is on average stronger (i.e., less efficiently screened) at $B=8$ T. This occurs because the electrons moving to screen the surface field experience a perpendicular force induced by the magnetic field and are consequently accelerated away from the direction of the surface electric field. This makes their screening action less efficient. As a consequence, the larger the magnetic field, the weaker the screening of the surface field (see Fig. 4). It should be remembered that most of the energy of the THz pulse is released during the first cycle of the pulse with duration of about 1 ps. It is thus evident that a reduction in screening over this time scale can contribute to the enhancement of THz emission observed in the presence of the magnetic field at high excitation densities.

From fits in Figs. 1 and 4 the parameter value $b=0.8$ is obtained.[21] By using Eq. (2) the corresponding scattering angle can be calculated. As shown in Fig. 6, for all B values used in the experiment, $\theta_S<360°$, which implies that in the average carriers do not complete an entire cyclotron orbit. This is consistent with the fact that emission spectra measured on the same sample by electro-optic sampling (EOS) (shown in Fig. 6 inset) do not show any clear narrow cyclotron features.[22]

By using Eq. (1), the value of the scattering time as a function of the carrier density can also be extrapolated from experimental data. The value of τ calculated with $b=0.8$ is plotted as a solid line in Fig. 7 over the carrier-density range

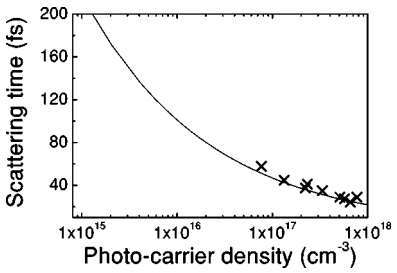

FIG. 7. Carrier-carrier scattering time as a function of the photogenerated carrier density. Solid line represents scattering time calculated from Eq. (1) with $b=0.8$, as obtained from fitting experimental data in Fig. 4. Symbols describe data reported by Portella *et al.*[19]

10^{15}-10^{18} cm^{-3}. In Fig. 7 we also show the data measured by Portella *et al.*[19] (symbols), who reported the first measurements of carrier-carrier scattering times in bulk GaAs as a function of the photogenerated carrier density. Portella *et al.* used a pump-probe technique to achieve a time-resolved measurement of the distribution of photoexcited carriers in the *k* space. Their measurements refer to high carrier densities in the range 8×10^{16}-8×10^{17} cm^{-3}, while ours are limited to 10^{14}-10^{16} cm^{-3}, but the two sets of data are in agreement. This is a significant confirmation of our assumption that carrier-carrier scattering is the predominant scattering mechanism in our experiment. Moreover, this proves that THz emission can be a powerful tool for the study of subpicosecond carrier dynamics, providing important informations such as carrier-carrier scattering time, which are not straightforward to measure otherwise.

In summary, we have presented an experimental study of the effect of optical fluence on THz emission from (100) GaAs in the presence of a magnetic field and compared our findings with both an analytical model and a Monte Carlo simulation. Different excitation regimes have been explored, showing different magnetic-field-related effects. In the case of *low* excitation densities ($n<n_{dop}$), an increasing magnetic field increases the carrier cyclotron frequency and scattering length. In the limit of *high* excitation densities ($n>n_{dop}$), in addition to carrier-carrier scattering, screening of the built-in surface field by photogenerated charges also occurs inducing saturation of THz power. The presence of a magnetic field reduces this saturation effect and so contributes to increase the emitted power. Monte Carlo simulations confirm that the magnetic field slows down the screening of the surface field by about 1 ps, which is comparable to the typical duration of the main cycle of the emitted THz pulse. In conclusion, it is seen that the optical fluence plays a key role in the enhancement of terahertz radiation in a magnetic field—a key issue largely ignored in previous studies.

The work was partially funded by the EPSRC (UK). EHL and AGD acknowledge support from the Isaac Newton Trust and the Royal Society, respectively.

*Corresponding author.

[1] B. B. Hu, J. T. Darrow, and D. H. Auston, Appl. Phys. Lett. **67**, 3523 (1995).
[2] Q. Wu and X.-C. Zhang, Appl. Phys. Lett. **56**, 886 (1990).
[3] C. M. Ciesla, D.D. Arnone, A. Corchia, D. Crawley, C. Longbottom, E.H. Linfield, and M. Pepper, Proc. SPIE **3934**, 73 (2000).
[4] P. Y. Han, G. C. Cho, and X.-C. Zhang, Opt. Lett. **25**, 242 (2000).
[5] M. Nuss and J. Orenstein, in *Millimeter and Submillimeter Wave Spectroscopy of Solids*, Topics in Applied Physics, Vol. 74, edited by G. Grüner (Springer-Verlag, Berlin, 1998), Chap. 2.
[6] P. N. Saeta, B. I. Greene, and S. L. Chuang, Appl. Phys. Lett. **63**, 3482 (1994).
[7] X.-C. Zhang and D. H. Auston, J. Appl. Phys. **71**, 326 (1992).
[8] R. McLaughlin, A. Corchia, M.B. Johnston, Q. Chen, C.M. Ciesla, D.D. Arnone, G.A.C. Jones, E.H. Linfeld, A.G. Davies, and M. Pepper, Appl. Phys. Lett. **76**, 2038 (2000).
[9] Hideyuki Ohtake, Shingo Ono, Masahiro Sakai, Zhenlin Liu, Takeyo Tsukamoto, and Nobuhiko Sarukura, Appl. Phys. Lett. **76**, 1398 (2000), and references therein.
[10] X.-C. Zhang, Y. Jin, T.D. Hewitt, T. Sangsiri, L.E. Kingsley, and M. Weiner, Appl. Phys. Lett. **62**, 2003 (1993).
[11] C. Weiss, R. Wallenstein, and R. Beigang, Appl. Phys. Lett. **77**, 4160 (2000).
[12] J. Shan, C. Weiss, R. Wallenstein, R. Beigang, and T. F. Heinz, Opt. Lett. **26**, 849 (2001).
[13] M. B. Johnston, D.M. Whittaker, A. Corchia, A.G. Davies, and E.H. Linfield, Appl. Phys. Lett. (submitted).
[14] S. R. Andrews (private communications).
[15] J. D. Jackson, *Classical Electrodynamics* (Wiley, New York, 1975), Chap. 14.
[16] D. Some and A. V. Nurmikko, Phys. Rev. B **50**, 5783 (1994).
[17] J. Shah, *Ultrafast Spectroscopy of Semiconductors and Semiconductor Nanostructures*, Springer Series in Solid-State Science, Vol. 115 (Springer-Verlag, Heidelberg, Germany, 1996), Chaps. 3–4 and references therein.
[18] G. Fasol, W. Hackenberg, H. P. Hughes, K. Ploog, E. Bauser, and H. Kano, Phys. Rev. B **41**, 1461 (1990), and references therein.
[19] M. T. Portella, J.-Y. Bigot, R. W. Schoenlein, J. E. Cunningham, and C. V. Shank, Appl. Phys. Lett. **60**, 2123 (1992).
[20] N. W. Ashcroft and N. D. Mermin, *Solid State Physics* (Saunders College, Philadelphia, 1976).
[21] This value is close to the case when two nearest-neighbor electrons move toward each by thermal motion; in this case they will collide after traveling over a distance $d/2=0.5n^{-1/3}$, which corresponds to $b=0.5$ in Eq. (1).
[22] E. Batke, K. Bollweg, U. Merkt, C. M. Hu, K. Köhler, and P. Ganser, Phys. Rev. B **48**, 8761 (1993).